EINDHOVEN UNIVERSITY OF TECHNOLOGY

Department of the Built Environment

Fire safety of bio-based insulation materials in sloping roofs with integrated PV-panels

by

K. Bekkers

MASTERPROJECT

Program:	Architecture building and planning
Supervisor:	ir. Ruud van Herpen FIFireE
Date:	28-03-2026
Student ID:	2042444
Study load (ECTS):	10
Track:	Building Physics and Services
Version:	2.0

Abstract

The energy transition promotes the use of bio-based insulation materials and the local generation of renewable energy. This is partly achieved using building integrated photovoltaics (BIPV). However, this in-roof system has limited ventilation possibilities, and the combination with combustible bio-based insulation materials, may lead to elevated cavity temperatures and an increased risk of fire.

Dutch building regulations prescribe reaction to fire requirements for roofs in relation to the external fire exposure. These requirements apply to both the external surface of the roof, and the roof construction as a whole. Fires that originate within the external separation construction itself and spread through this roof construction are not covered by these regulations, since materials within the roof, such as insulation materials and membranes, are not individually required to meet these reaction to fire requirements. This study aimed to determine maximum temperatures and evaluate fire risk in unventilated air cavities beneath BIPV panels. There is limited knowledge regarding the maximum temperatures that may develop in unventilated cavities underneath BIPV in sloped roof constructions with bio-based insulation materials in Dutch climate conditions.

To answer the research question, a literature review was conducted in combination with analytical calculations and both steady-state and transient simulations. The simulations were performed using the Voltra 8.1. thermodynamic software. The following assumptions were used for the calculations: a sloped, south-facing roof of 35° with an unventilated air cavity of 45 mm was modelled. From the interior to the exterior, the structure consists of roof boarding, insulation, an air cavity, and BIPV. The thickness of the insulation material was adjusted to achieve a thermal resistance of 6.3 m²K/W. External temperature and solar irradiance were applied under both constant and dynamic conditions. A reduced heat transfer coefficient was used to represent low wind conditions.

The results indicate that bio-based insulation slightly reduced cavity temperatures due to higher heat capacity compared to plastic insulation material. PIR insulation reached the highest temperatures with a difference of approximately 4°C. Wood fibre insulation, with an ignition temperature of 100-130°C, approached the calculated air cavity temperatures under the worst-case conditions, indicating a potential fire risk. Based on these findings, the unprotected use of wood fibre insulation in the air cavity requires careful consideration. The results highlight the importance of careful material selection, especially when combustible materials with low ignition temperatures are applied. Besides the material selection, this research underlines the beneficial effect of ventilation beneath PV-panels, as ventilation enhances heat dissipation and improves the efficiency.

Table of Contents

1. Introduction

The energy transition is a response to the increasing concentration of greenhouse gases in the atmosphere, aiming to shift from a linear to a circular economy. This transition involves replacing fossil fuels with renewable energy sources and substituting non-renewable materials with secondary materials and carbon-neutral biomass (Circle Economy, 2025). Within the built environment, this transition leads to an increase in the local generation of solar energy using photovoltaic panels (PV).

In residential buildings, PV panels are installed either on the roof as building-applied PV (BAPV) or in the roof as building integrated PV (BIPV). In BAPV, the insulation material is shielded by the cladding material of the building envelope. In contrast, BIPV panels are integrated into the building envelope, typically resulting in a limited separation between the PV system and the underlying insulation material (Nederlands Instituut Publieke Veiligheid, 2025).

In addition, the use of bio-based insulation materials is increasing. These materials can be produced from carbon-neutral biomass, contributing to the circular economy. However, these materials react different to fire compared to conventional insulation materials such as glass wool, PIR, PUR, EPS, and non-combustible rock wool insulation (RVO, 2022). The introduction of a new energy system, which is placed within the building envelope, combined with combustible bio-based insulation materials increases the risk of fire.

Innovations are developing faster than changes in legislation and regulations (J. Reinders et al., 2023). In the current Dutch building regulations, fire-resistance requirements apply exclusively to the exterior of the roof. This exterior must not pose a fire hazard and is assessed using a fire brands test. Materials within the roof, such as insulation materials and membranes, are not required to meet fire-resistance criteria. Meanwhile, the Dutch Organisation for Applied Natural Science Research (TNO) has conducted an inventory of fire incidents involving PV systems. These results indicate that, from a relative perspective, a higher number of fire incidents have been reported in buildings with installed BIPV compared to BAPV (E.E. Bende & N.J.J. Dekker, 2019).

A south-facing sloped roof surface captures the highest level of solar radiation. PV panels integrated into the building envelope have a reduced heat dissipation compared to PV panels on top of the building envelope, due to limited ventilation possibilities. This may result in elevated temperatures within the cavity, directly above the insulation material (AgentschapNL, 2011). Previous tests conducted by Nieman have shown that wood fibre insulation has a relative low ignition temperature and can ignite at temperatures between 100 and 130 °C. If temperatures within the cavity approach or exceed these values, there may be potential risk of fire (RVO, 2022).

Currently, there is limited knowledge regarding the maximum temperatures that may develop in unventilated cavities underneath BIPV in sloped roof constructions with bio-based insulation materials under Dutch climate conditions. It remains unclear whether the thermal properties of bio-based insulation material have a positive influence on the temperature within the air cavity, or whether cavity temperatures may approach or exceed the ignition temperature of the material, thereby increasing the risk of fire. The aim of this study is therefore to determine the maximum cavity temperature and to evaluate the risk associated with the application of bio-based insulation materials in sloped roof structures with BIPV panels in the Netherlands.

The main research question of this study is:

What is the influence of bio-based insulation materials on the fire risk in an unventilated air cavity in a sloping roof with building integrated photovoltaics?

To answer the main question of this research, a literature review was conducted. This review identified fire risks associated with recent building developments and PV installations. In addition, the ignition behaviour of traditional insulation materials, such as rock wool and PIR, were analysed and compared with two bio-based insulation materials, wood fibre, and cellulose. Heat transfer within the roof was analysed through analytical calculations and simulated using the Voltra simulation program developed by Physibel. In this study, the maximum cavity temperature was determined under a defined worst-case scenario.

The structure of the report is as follows. Chapter 2 contains a literature review, Chapter 3 describes the research methodology. Chapter 4 presents the results of the calculations, the findings are discussed in chapter 5 and Chapter 6 presents the conclusion of this study.

2. Literature review

The increasing application of PV panels on residential buildings may influence the fire safety performance. BIPV panels combined with bio-based insulation materials have not yet been widely applied but may become more common in the future. This combination is currently permitted under existing Dutch building legislation and regulations. However, the adequacy of existing regulatory frameworks, for addressing new innovations, remains a subject of debate. This chapter provides an overview of relevant literature associated with the key concepts of this study.

2.1. Fire safety for sloping roof structures with BIPV

2.1.1. Performance-based versus regulation-based approaches

Current fire safety legislation and regulations consist of previously approved rules. Compliance with these regulations can be assessed with minimal need for further discussion. This is due to the clear and transparent laws and regulations. This method of assessment is referred to as a regulation-based approach. A limitation of this approach is that it is largely based on historical data and past incidents. The introduction of innovations may introduce new fire risks for which existing regulations are insufficiently prepared. In addition, buildings are becoming increasingly complex, and factors such as occupant characteristics and the presence of combustible materials play an important role in the overall fire safety. Adjustments to legislation and regulations are a long-term process, resulting in innovations being introduced more rapidly than the applicable laws and regulations can adapt (R. van Liempd et al., 2024). Furthermore, new introduced legislation and regulations typically apply to new buildings only, while existing building are not required to comply with them. It is therefore important to identify the potential risks that extend beyond the existing legislation and regulations to ensure an adequate level of safety (Veiligheidsregio Haaglanden, 2024).

2.1.2. Regulations for sloping roof structures

There are no fire resistance requirements for external separating constructions, such as the sloping roof surface considered in this study. However, there are requirements regarding fire behaviour. This fire behaviour is assessed by exposing the construction to fire-brands and limited heat radiation. NEN 6063 evaluates the impact of the external fire and radiation on the roof construction as a whole. In contrast, NEN 6069 assesses the outer surface of the roof to determine the fire classification of the external construction element. Fires that originate within the external partition structure itself and spread through the construction are not covered by these regulations. This includes, among other things, the use of BIPV systems, which may function as an ignition source within the building envelope. As current legislation and regulations do not specifically address this issue, BIPV systems can be applied in combination with combustible (bio-based) insulation materials. This introduces not only a potential ignition source into the construction, but also additional fuel due to the presence of combustible insulation materials. Although various guidelines encourage the safe use of BIPV systems, it is not mandatory to follow these guidelines unless specifically prescribed.

2.2. Fire behaviour of insulation materials

2.2.1. Traditional insulation materials

The fire safety risks associated with traditional insulation materials have been extensively studied. Rock wool insulation is one example of a traditional insulation material and has an ignition temperature of approximately 1100°C (S. Baaij et al., 2023). Rock wool insulation is a non-combustible according to NEN-EN 13501-1, with negligible smoke production and limited toxic gas emissions. Synthetic insulation materials such as PIR (polyisocyanurate) and PUR (polyurethane) are widely used due to their low thermal conductivity, allowing high insulation levels to be achieved with limited thickness. These materials are also lightweight and relatively inexpensive. However, these materials exhibit a lower ignition temperature (above 250°C) and may contribute to fire growth by releasing toxic gases and melting during combustion (Giunta d'Albani et al., 2017).

2.2.2. Bio-based

Bio-based insulation materials are increasingly being applied in building construction. These materials can be produced in a carbon-neutral manner, thereby supporting the circular economy. Since it is impossible to be completely dependent on secondary materials, carbon-neutral insulation materials are needed for achieving the circular economy goals (Circle Economy, 2025). Bio-based insulation materials generally have a higher specific heat capacity compared to traditional insulation materials. A higher heat capacity results in a greater thermal phase shift. This means that it takes longer for a material to heat up, resulting in a reduced risk of overheating and temperature fluctuations (Lente-Akkoord Circulair Industrieel Bouwen, 2024). However, bio-based insulation materials are composed of organic materials and are flammable without fire-retardant additives. Research conducted by Nieman on behalf of Building Balance has investigated the fire behaviour of various bio-based insulation materials. The findings show that, in the presence of an external ignition source, wood fibre insulation can undergo piloted ignition at relatively low temperatures, between 100-130°C. Cellulose insulation, in contrast, ignites at temperatures between 250°C and 400°C. It should be noted that approximately 8% fire retardant additives have been added to this insulation material (RVO, 2022). The fire resistance of these bio-based insulation materials can be improved by adding fire-retardant salts or by wrapping the insulation material in fire-resistant cladding. However, chemical fire retardants additives contain substances that are harmful to the environment and public health.(Maksym Li et al., 2025)

In addition to their flammability, bio-based insulation materials can also smoulder. Smouldering is a slow combustion process that can occur at elevated temperatures. It is a flameless combustion process, which makes it difficult to detect. The temperature of smouldering insulation material is between 300°C and 400°C, depending on the oxygen concentration. At oxygen concentrations below 12%, insufficient oxygen concentration is available to sustain the smouldering (Sudhoff, 2024). Insulation materials can reignite even after a fire has been extinguished. Because this smouldering behaviour is difficult to detect, it can continue unnoticed within the structure for an extended period, potentially causing greater damage than the initial fire (Clarion Events North America, 2000).

Bio-based insulation materials undergo charring during combustion. This can be considered as beneficial property compared to plastic-based insulation materials, which melt or release flammable gases when exposed to high temperatures. However, it is important that the insulation material remains secured in place and is not directly exposed to extreme temperatures or flames. This can be achieved by using, for example, a protective sheet material.

2.3. PV systems and fire safety

The installation of a PV system on a roof introduces an additional fire risk. PV systems can be installed either on the roof as BAPV or in the roof as BIPV. In BAPV systems, the PV panels are located on the building envelope, creating a physical (potentially non-combustible) barrier between the PV panel and the underlaying insulation material. Because the system is installed on the roof, there is generally a ventilated air gap between the panels and the roof surface. This helps to dissipate heat and has a positive effect on the efficiency. A BIPV system may be preferred from an aesthetic point of view, or to reduce material use and construction costs. In a BIPV system, the PV panels are integrated into the building envelope and are often placed directly above the insulation layer, depending on the roof structure and the type of PV system used. As a result, there is often limited ventilation space between the PV panels and the underlying material. This can result in limited heat dissipation, which has a negative effect on efficiency. For every degree Celsius increase, the efficiency decreases by approximately 0.45% (AgentschapNL, 2011). Research comparing BIPV with BAPV systems indicates that BIPV systems have a fire risk that is up to twenty times higher than that of BAPV systems (Hemann Laukamp et al., 2013).

Fires in PV systems can be initiated either by an external fire or by a technical failure within the PV system itself. In many cases, incidents result from a combination of different causes and circumstances, involving both technical and human factors. A significant proportion of the fire incidents investigated by TNO occurred at relatively high temperatures, with elevated solar radiation and mainly low wind speeds. Furthermore, incidents appear to occur more frequently when connectors from different manufacturers are combined or when installation components are improperly secured (E.E. Bende & N.J.J. Dekker, 2019).

PV panels capture solar radiation in direct current, which is converted to alternating current by the inverter. Because of the presence of direct current, electrical faults are more likely to cause a sustained arc rather than a short circuit. This sustained arc increases the risk of ignition of underlying combustible materials (R. van Herpen, 2022).

Installation guidelines for PV panels often specify the use of a membrane with a fire-resistance classification of class A or B. These membranes are designed to withstand higher air temperatures. However, in the occurrence of thermal hotspots (localised overheating) combined with limited ventilation, the maximum temperature of these standard membranes may be exceeded and increasing the risk of fire (Nederlands Instituut Publieke Veiligheid, 2025). Besides membranes under PV panels, there are also double-glazed PV panels. These have a lower risk of back sheet degradation, last longer, and reduce the risk of fire because the combustible membrane is replaced with non-combustible glass (Zhang et al., 2015).

2.4. Solar radiation

Solar radiation is typically expressed in W/m² and varies across different regions on Earth. This variation is primarily due to the tilt of the earth's axis and its elliptical orbit around the Sun. In the northern hemisphere, the highest levels of solar radiation are observed in June and July. South-facing roof surfaces receive the highest level of solar radiation (Velds, 1992). Research conducted by abt-consultants shows that an angle of inclination of 35° is optimal for solar panels in the Netherlands (Ir. H.G. Krijgsman & Ir. R.H.G. Roijakkers, 2021). Under conditions of high solar irradiance, BIPV may experience significant thermal loading.

2.5. Fire in the air cavity

In an open-fire scenario, heat is released into the surrounding environment through convection and radiation. In contrast, a fire occurring within an air cavity traps heat and combustible gases between two parallel surfaces, resulting in higher temperatures within the cavity. This can contribute to an increased fire spread and may result in temperatures which exceed the standard fire curve. In addition, the increased temperature causes a strong upward flow, known as the chimney effect or stack effect, which encourages the spread of fire (Godakandage et al., 2023). Although this research does not model active fire scenarios, these findings illustrate the potential consequences if a fire occurs within a cavity. This risk is especially critical for materials with a low ignition temperature, where a small spark can ignite large amounts of combustible material.

2.6. Summary of literature findings

Based on the reviewed literature, it can be concluded that, although fire behaviour of insulation materials and PV-related fire incidents have been studied separately, limited attention has been given to temperature development in unventilated cavities behind BIPV while using bio-based insulation materials under Dutch climate conditions.

3. Methodology

This chapter provides an overview of the principles and modelling approach used in the analytical calculations and numerical simulations.

3.1. Software

In this study, the temperature distribution within the air cavity was determined using the Voltra 8.1 software. Voltra is a simulation program developed by Physibel that enables the modelling of transient three-dimensional heat transfer. The VVMOD steady state airflow model was used to simulate the airflow that develops within the air cavity as temperatures increase.

3.2. Roof Structure and materials

Figure 1 illustrates the roof structure* used in the simulations. From the interior to the exterior, the structure consists of roof boarding, insulation, an air cavity, and BIPV. Only the insulation material was varied in the different calculations. The thickness of each insulation material was modelled such that a thermal resistance of 6.3 m²K/W was achieved , corresponding to the minimum thermal resistance required by Dutch building regulations for roof structures adjacent to the external environment. Within the simulations, traditional insulation materials (rock wool and PIR) were compared with two bio-based insulation materials (wood fibre and cellulose). Table 1 presents the properties of the materials.

*Battens and laths were not included in the simulation model.

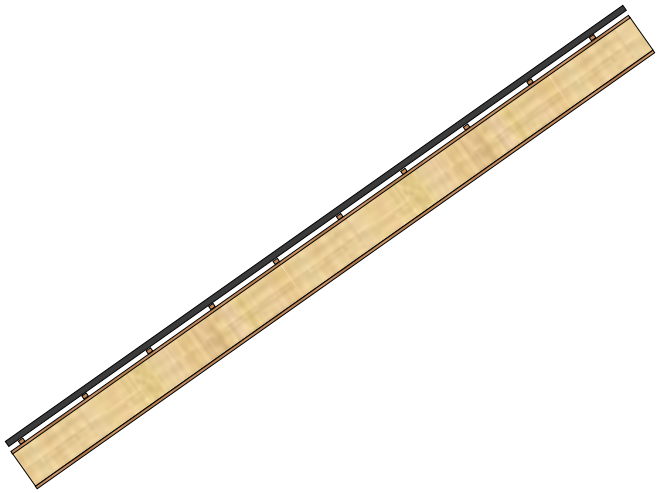

Figure 1: roof structure

Table 1: Properties and thermal conductivity of the materials

Material	Thickness [mm]	Thermal conductivity λ [W/(mK)]	Specific heat capacity [J/kgK]	Flammability [°C]
PV panel	40	1.000	1500	
Wood fibre insulation	265	0.042	2100	100-130
Cellulose	240	0.038	2100	250-400*
Rock wool	220	0.035	1000	1100
PIR	158	0.025	1200	>250
Wood	18	0.170	1880	

*with approximately 8% fire retardant additives

3.3. Analytical calculation

The temperature beneath the PV panels was determined under both steady-state and transient conditions.

The temperature within the air cavity was first calculated analytically to estimate the maximum temperature that could occur under specified boundary conditions. The standard surface heat transfer resistance of 7.7 W/m²K, according to the NEN 1068, was applied for the indoor air boundary. The cavity was assumed to be unventilated, with a thermal transmittance of 0.17 W/m²K. The external surface heat transfer coefficient is assumed to be lower than the standard value specified in the NEN 1068. This adjustment is made because the conventional transition resistance of 25 W/m²K only occurs in situations with high wind speeds. However, this study considered a worst-case scenario in which the external wind speed is assumed to be limited, resulting in a reduced heat transfer. The external surface heat transfer coefficient is reduced to 13.5 W/m²K, thereby limiting heat transfer between the structure and the outside air. For the PV panels, wood fibre insulation and the wooden roof boarding, the thicknesses and thermal conductivity values presented in table 1table 1 have been used. An indoor air temperature of 30°C and an external temperature of 35°C were assumed. A constant solar irradiance of 1000 W/m² was applied to the exterior surface. A surface absorptivity of 0.9 was assumed for the materials.

The external surface of the structure is heated by the air temperature and solar radiation. A steady-state condition is assumed, in which the flow through the structure equals the outflow from the structure. The external surface temperature of the structure is determined using equation 01.

$$e * q_{rad} + h_a * (T_a - T_{ao}) - \frac{T_{ao} - T_{io}}{R_c} - h_i(T_{io} - T_i) = 0 \qquad (01)$$

The thermal resistance of the materials was determined based on their thickness and thermal conductivity, as presented in table 2.

Table 2: Materials and thermal conductivity

	Thermal conductivity λ [W/(mK)]	Thickness [mm]	Rd [m²K/W]
integrated pv panels	1.000	40	0.040
cavity (unventilated)	0.212	36	0.170
wood fibre insulation	0.042	265	6.310
wood	0.170	18	0.106

Solving equation 01 gives 100.11°C for the external surface temperature and 31.39°C for the internal surface temperature. The complete calculation can be found in appendix 1.

The heat flow through the construction is determined using equation 02.

$$q = \frac{(T_{oa} - T_{io})}{R_c} \qquad (02)$$

The calculated heat flux through the construction is: 10.37 W/m².

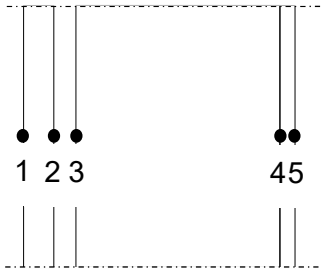

Figure 2: Schematic representation of the construction layers from the exterior to the interior.

At the outside of the insulation material (junction 3, as can be seen in figure 2), the temperature is determined using equation 03. For this calculation, the thermal resistances of the layers up to this junction (determined in table 2) are summed.

$$T_{outside\ insulation} = T_{ao} - q * \sum_{i=3}^{j} R \qquad (03)$$

This results in a temperature of 97.2°C on the external surface of the insulation layer. In this calculation, the outer surface of the insulation layer is the determining factor since the temperature decreases deeper within the construction.

3.4. Voltra simulation

In Voltra, a steady state calculation was first performed, which could be directly compared with the analytical calculation. This calculation was subsequently extended to a transient (more realistic) simulation, in which the solar radiation on the exterior surface (and the external air temperature) were based on measured climate data from De Bilt. The advantage of this transient analysis is that it enables the influence of the heat capacity of the different materials on the temperature development within the air cavity to be investigated. The following paragraphs first describe the parameters that are the common to both the steady state and transient simulations. This is followed by a description of the parameters that are specific to either the steady state or the transient simulation.

3.4.1. Boundary conditions

Outdoor air

Under high wind conditions, the external convective heat transfer coefficient is typically 25.00 W/m²K. In this study, a worst-case scenario with a low wind speed was assumed, resulting in a reduced external heat transfer coefficient. Therefore, a value of 13.50 W/m²K was applied.

Cavity

Within the air cavity, radiative heat transfer has the greatest influence on temperature exchange (see figure 3). Solar radiation on the exterior surface was modelled with a surface absorption of 0.9, meaning that 90% of the radiation was absorbed and 10% was reflected. To determine the temperature within the air cavity, both convection and radiative heat transfer were calculated. This was achieved by assigning the air cavity to the BC_FREE boundary condition. This boundary condition represent an unventilated air cavity for which the convective heat transfer coefficient has been calculated. Heat transfer occurred from the heated external surface, exposed to high temperatures and strong solar radiation, toward the cooler internal surface. As a result, the given heat flow was oriented along the z-axis and calculated in the downward direction (CEN_Zy_I). Three C-values were applied to describe this heat flow direction. C1 = 0.025, C2 = 0.09*d-0.44, C3 = 0.187. An air cavity height of 0.045 m was applied, resulting in a C2 value of 0.3522.

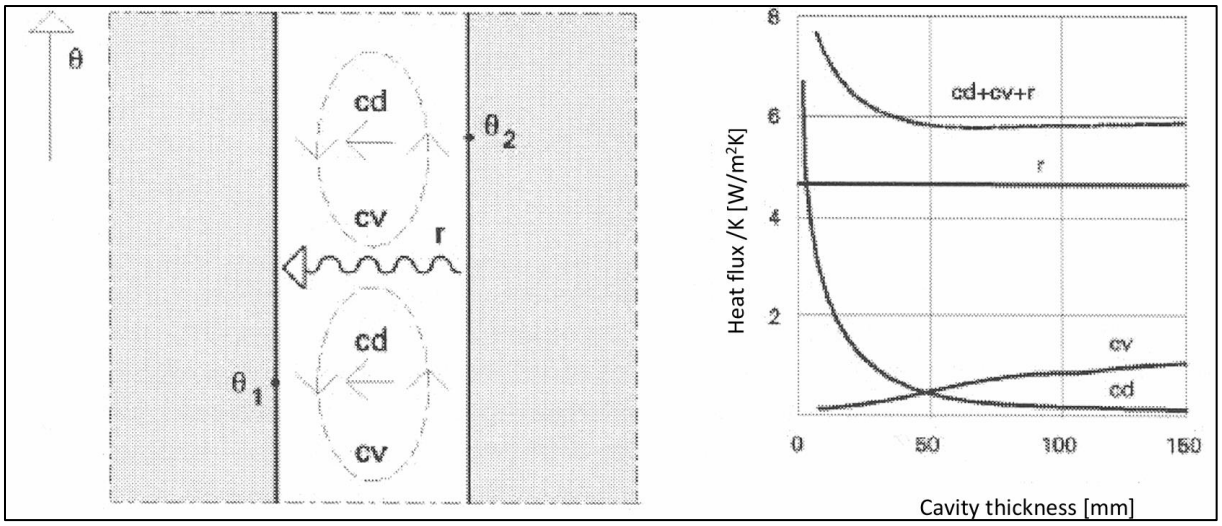

Figure 3: Heat transmission in cavity (Thijs van Druenen, 2025)

Indoor air

For the indoor environment, an air temperature of 30°C was assumed and a standard heat transfer coefficient for the Netherlands of 7.7 W/m²K was applied.

Materials

The material properties and the thermal properties of the air layers are summarized in table 3. The insulation material is highlighted in grey, as it varies between the different simulations.

Table 3: Boundary conditions materials

Layer	Type	CEN-rule	lambda [W/mK]	α [-]	density [kg/m³]	specific heat capacity [J/kgK]	T [°C]	h [W/m²K]	C1	C2	C3	Sun	ρ [-]	τ [-]
Outside air	BC_SIMPL	NIHIL					T01	13.50				YES		
Cavity	BC_FREE	CEN_Zy_I			1.2	1000.0			0.025	0.352	0.187			
PV			1.000	0.90	1500.0	1500.0							0.10	0.00
Wood fibre			0.042	0.90	40.0	2100							0.10	0.00
Cellulose			0.038	0.90	50.0	2100							0.10	0.00
Rock Wool			0.035	0.90	70.0	1000							0.10	0.00
PIR			0.025	0.90	30.0	1200							0.10	0.00
Fibreboard			0.170	0.90	700.0	1880							0.10	0.00
Inside air	BC_SIMPL	HI_NORML					30.0	7.70						

3.4.2. Steady state simulation

In the steady state simulation, a constant solar irradiance of 1000 W/m² was applied on the roof surface. In addition, a constant outside air temperature of 35°C was maintained as a boundary condition.

3.4.3. Transient simulation

Two scenarios were investigated within the transient simulation. In the first scenario, solar radiation was applied dynamically with a constant temperature of 35°C (see figure 5). In the second scenario, both solar radiation and outdoor air temperature were implemented as dynamic boundary conditions (see figure 6). This approach enabled the evaluation of the cavity temperature based on historical climate data and the thermal performance of different insulation materials under transient conditions. The following sections describe how the data was obtained and verified.

Solar radiation

The solar irradiance applied to the roof surface was based on climate data provided by Physibel. This data was verified by measurement data from the KNMI, collected between 1951 and 1980 (Velds, 1992). According to the KNMI, solar radiation levels have been increased by 15% between 1980 and 2025. This increase is attributed to reduced air pollution, which is the result from stricter environmental regulations, which allows more solar radiation to reach the earth (KNMI, 2025). In order to incorporate this increased solar radiation into the simulation, the data from the measurement were multiplied by a factor of 1.15, before implementation in the simulation. Appendix 2a presents the maximum solar radiation per month, while Appendix 2b shows the data including an additional 15% safety margin. These values were compared with the Physibel solar global and diffuse radiation.

Figure 4 presents the solar radiation curve derived from the measurement data (including the applied safety margin of 15%) in comparison with the data provided by Physibel. This shows that Physibel's solar data is active at a smaller interval. However, similar maximum solar radiation is achieved. Although the Physibel data does not show the highest solar radiation throughout the day, the Physibel data was preferred because direct and diffuse radiation components can be specified separately. The roof surface was modelled at an angle of 35°, after which Voltra automatically calculated the direct and diffuse solar radiation on the surface.

Scenario 1: Temperature constant

In the first scenario, a constant outdoor temperature of 35 °C was applied. Although such a temperature does not remain constant throughout the day in the Netherlands, it gives an indication of the maximum temperatures that can be reached in the air cavity in the worst-case scenario.

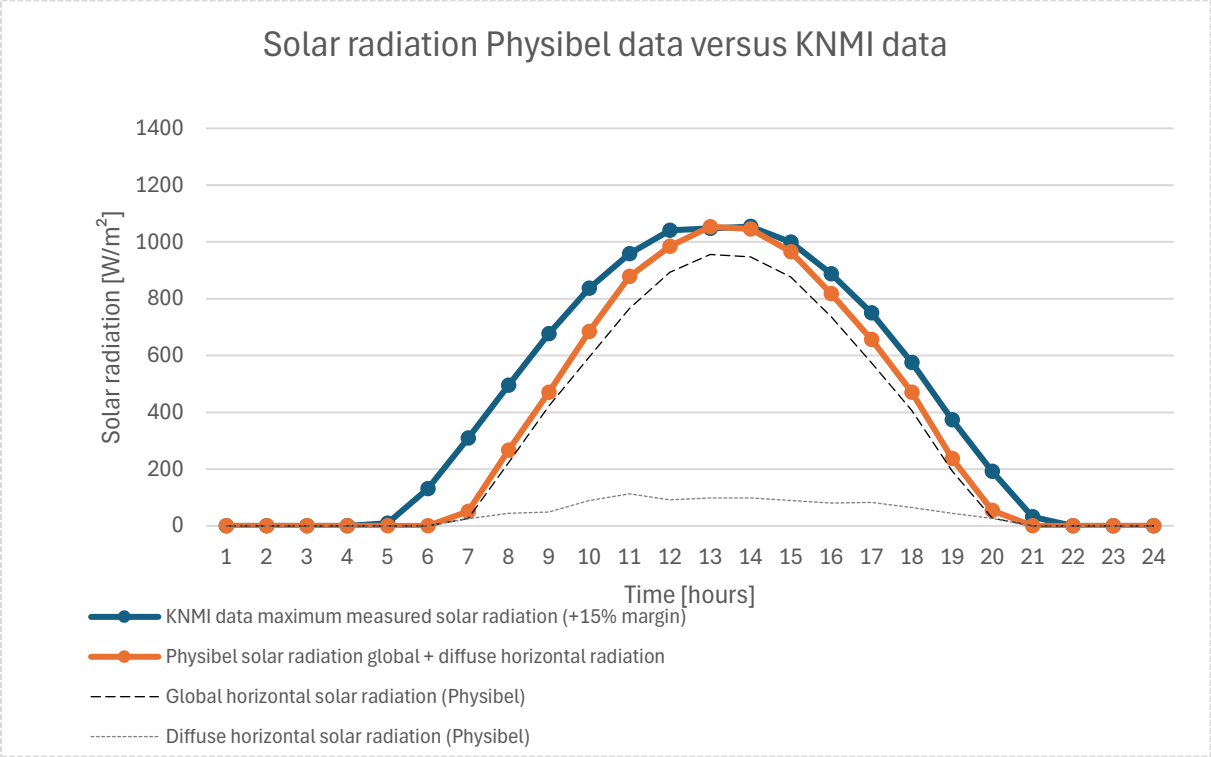

Figure 4: Solar radiation KNMI vs Physibel data

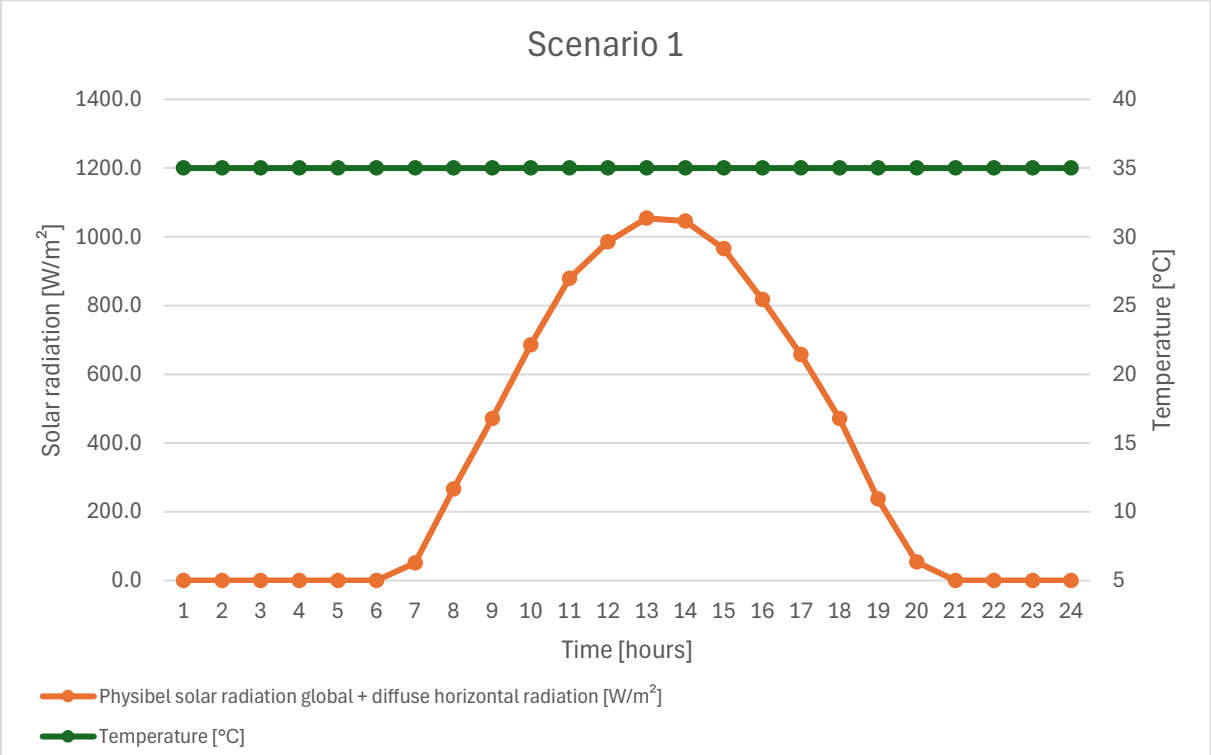

Figure 5: Input data Voltra scenario 1

Scenario 2: temperature dynamic

In the second transient simulation, both outdoor temperature and solar radiation were implemented as dynamic inputs based on Physibel's climate data. The day with the highest recorded solar radiation combined with a high air temperature was selected as input for the simulations. This corresponds to day 230 (see appendix 3). The simulation was performed to evaluate the first transient simulation, in which a constant external air temperature was used. The second transient simulation does not represent a worst-case scenario. Nevertheless, it enables the determination of cavity temperatures based on historical climate data and allows the impact of temperature variations throughout the day.

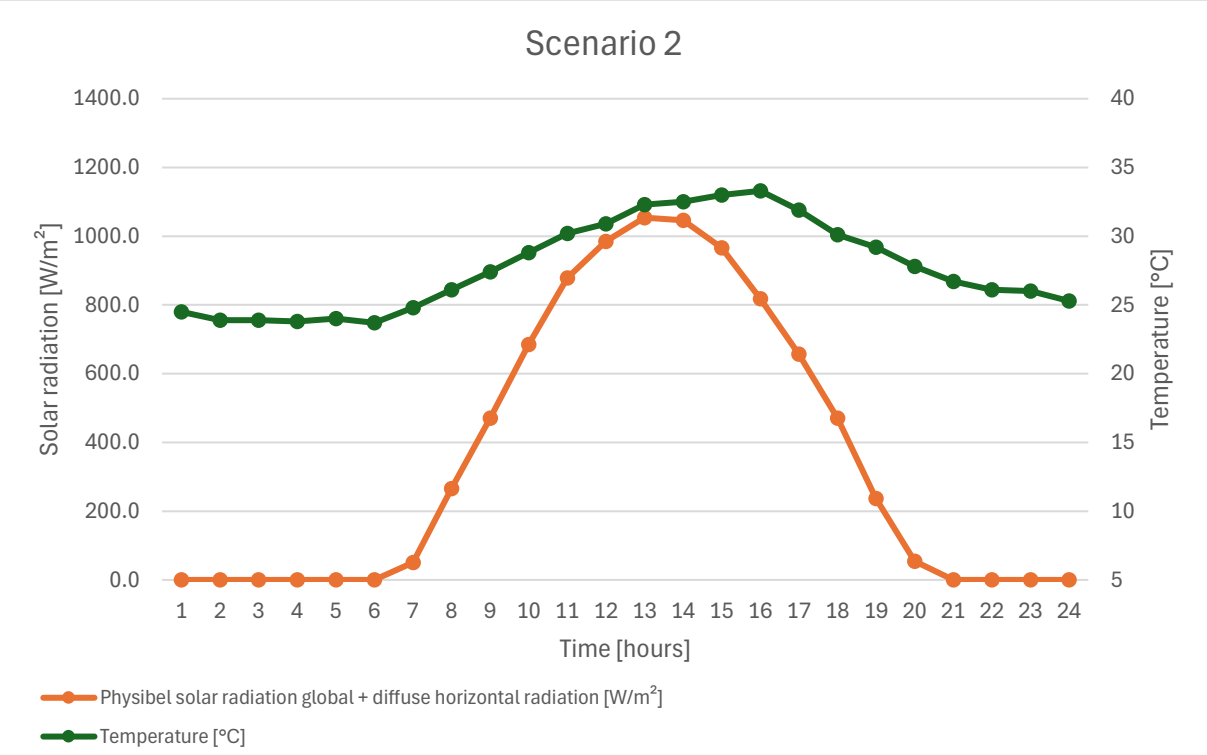

Figure 6: Measurement data for day 230, used in scenario 2

3.5. Assumptions and worst-case definition

This study was based on several modelling assumptions to define a conservative boundary condition and to isolate the influence of insulation material properties on the cavity temperature. The following assumptions were applied:

- The roof surface was assumed to be south orientated with a slope of 35°. This optimal orientation and angle were used to receive the highest levels of solar radiation;
- The air cavity beneath the BIPV was modelled as unventilated, with a cavity height of 45 mm;
- Battens and laths were not used in the calculation;
- A surface absorptivity of 0.9 was assumed for the materials;
- Solar radiation was modelled based on climate data provided by Physibel;
- A reduced external heat transfer coefficient of 13.5 W/m²K was applied, representing low wind speed conditions;
- Heat generation from reduced PV efficiency at higher temperatures was not included in the simulations;
- Insulation materials varied in thickness because each insulation material was modified such that a thermal resistance of 6.3 m²K/W was achieved;
- Scenario 1 assumed a constant temperature, while the simulations in scenario 2 assumed a dynamic temperature.

4. Results

The aim of this study was to determine the temperature within the air cavity beneath BIPV panels. The temperature was evaluated at the most critical location, namely at the external surface of the insulation material. At this location, the insulation material experiences the highest heating due to the external air temperature and solar radiation. The air temperature in air cavity was determined using both an analytical calculation and Voltra simulations.

4.1. Analytical calculation

The air cavity temperature was determined analytically. Based on the boundary conditions and material properties specified in Chapter 3, the calculated external surface temperature of the insulation reaches a temperature of 97.2°C.

4.2. Voltra simulation

4.2.1. Voltra steady state simulation

In the steady state simulation in Voltra, the temperature in the air cavity was determined under a constant solar radiation of 1000W/m² and a constant outdoor air temperature of 35°C. Based on the boundary conditions and material properties specified in Chapter 3, a temperature of 105.4°C was obtained at the outside of the insulation. The effect of different insulation materials on the temperature in the air cavity was not investigated in the steady state simulation. Because the solar radiation and the external temperature were constant, comparable temperature profiles for different insulation materials will be obtained. An overview of the imported Voltra data is provided in appendix 4.

Figure 7: Roof structure in Voltra

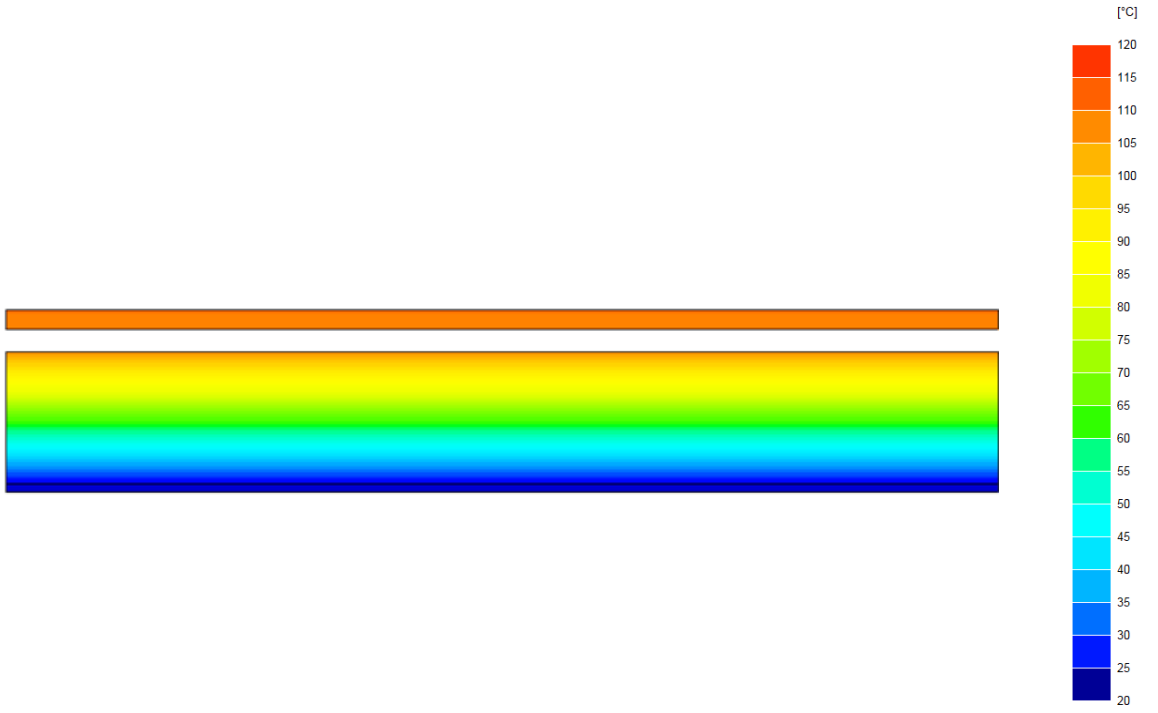

Figure 8: Temperature distribution through the roof structure

4.2.2. Voltra scenario 1

In the first Voltra scenario, dynamic solar radiation, as presented in chapter 3.4 figure 6, was included in the model. A worst-case constant external air temperature of 35°C was applied. The resulting temperatures at the external surface of the insulation material are presented in figure 9. The highest maximum temperature (110.0°C) was observed for PIR insulation. Figure 10 presents a comparison of the maximum temperatures for the different insulation materials. The maximum temperatures for cellulose, Wood fibre, PIR, and rock wool were 106.3 °C, 106.7 °C, 110.0 °C, and 107.9 °C.

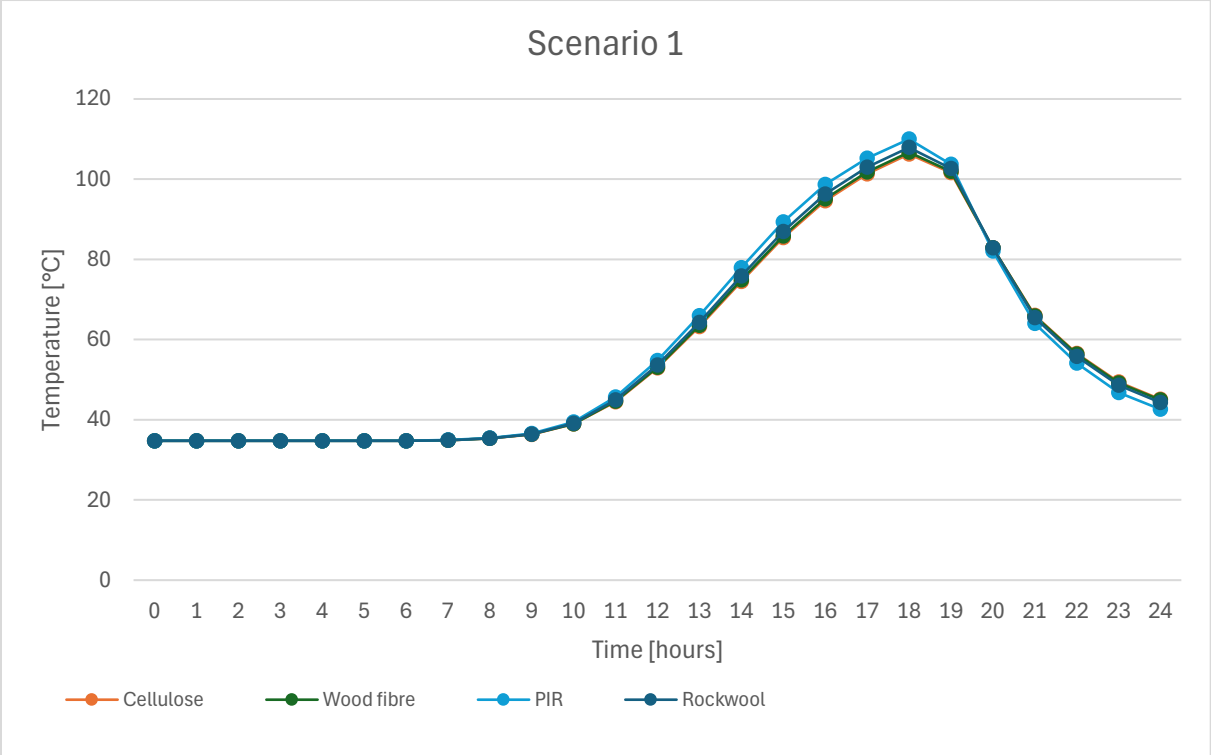

Figure 9: Simulation results scenario 1

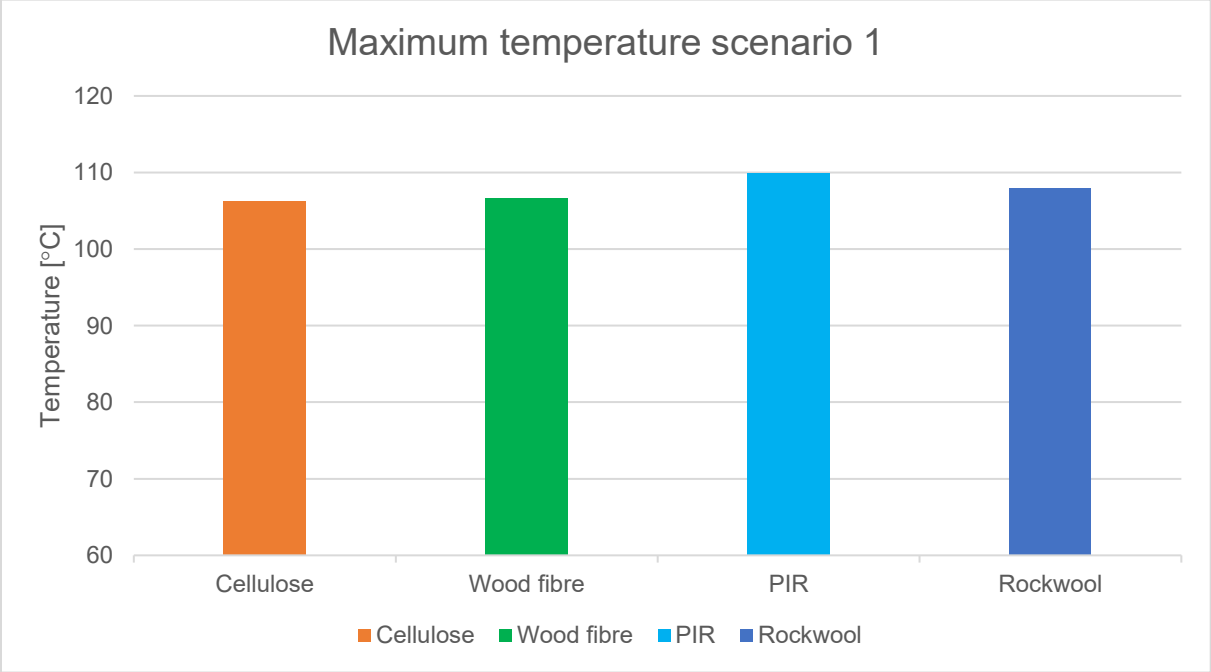

Figure 10: Maximum reached temperatures, scenario 1

4.2.3. Voltra scenario 2

The second Voltra scenario simulations used measured climate data provided by Physibel. The warmest day with the highest solar radiation from this database was selected for simulation. Both solar radiation and external air temperature were implemented as transient boundary conditions. This made it possible to evaluate whether different insulation materials have an influence on temperature development and the maximum air cavity temperature. Figure 12 present a comparison of the maximum temperatures between the different insulation materials. The maximum temperatures for cellulose, Wood fibre, PIR, and rock wool were 80.3 °C, 80.7 °C, 83.8 °C, and 81.8 °C.

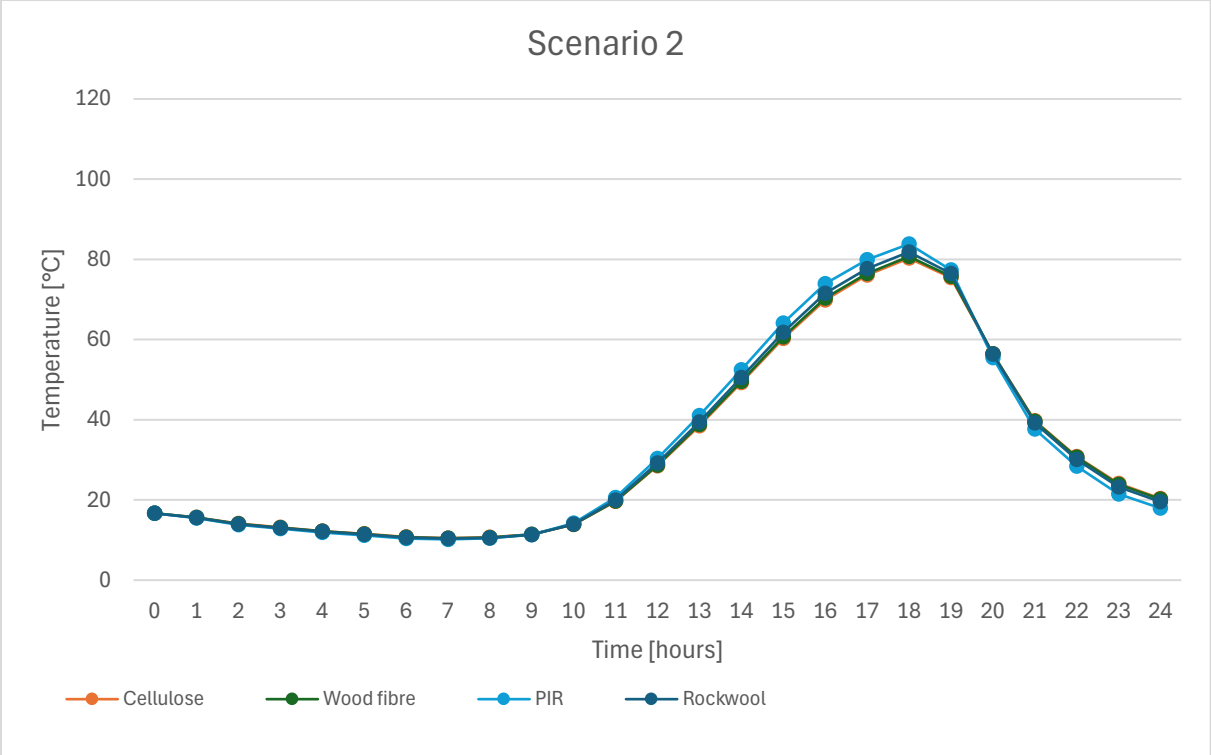

Figure 11: Voltra simulation results scenario 1

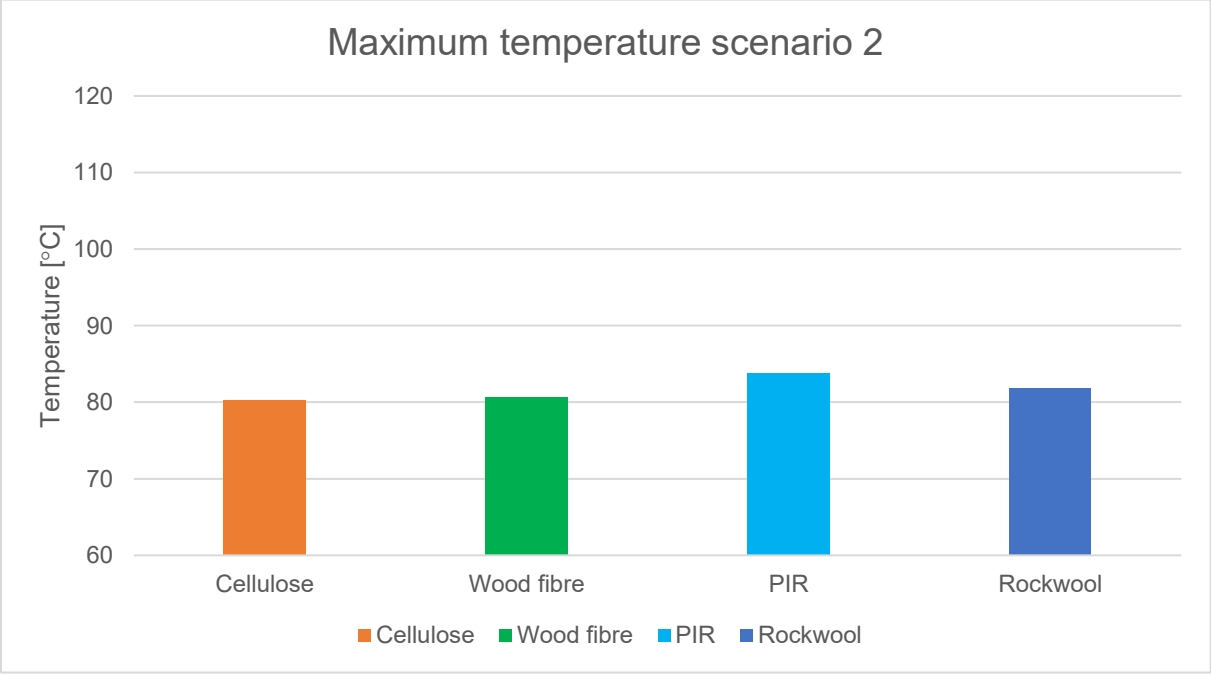

Figure 12: Maximum reached temperatures, scenario 2

5. Discussion

This study investigated temperature development at the exterior surface of insulation material located within an air cavity behind BIPV panels. The air temperature was calculated for different insulation types under various boundary conditions and solar exposure levels.

First, the analytical calculation was compared with the steady state simulation performed in Voltra. The results of the analytical calculation resulted in a lower maximum temperature. This difference can be related to the multiple boundary conditions applied to the air cavity. In Voltra, heat exchange within the air cavity is based on different interacting parameters. On the other hand, the analytical calculation applies standardised values for a simplification of the calculation, which may explain the lower obtained temperatures in the analytical calculation. To ensure that the correct boundary conditions were applied in the simulation model, the model developer was consulted, and the surface resistances and boundary conditions were reviewed and confirmed.

In the dynamic simulations, the results indicates that the selection of insulation material affects the temperature development in the air cavity. However, the differences between bio-based and traditional insulation materials are limited. In both scenarios, where dynamic solar radiation (and temperature) were applied, the highest air cavity temperatures among different insulation material varied by only 3-4°C. The highest air cavity temperature was observed for PIR insulation, whereas cellulose resulted in the lowest air cavity temperatures. Bio-based insulation materials showed nearly identical temperature development, which can be attributed to their comparable heat capacities. Although the heat capacity of PIR (1200 J/kgK) is higher than the heat capacity of rock wool (1000 J/kgK), the application of rock wool resulted in lower air cavity temperatures. The lower thermal conductivity of rock wool requires a greater insulation thickness to achieve the same thermal resistance, which influences the heat storage capacity.

The high temperatures in the air cavity affect the performance of the PV panels. The efficiency decreases by 0.45% per °C increase in temperature. At higher operating temperatures, the risk of malfunctions and additional heat generation in the panel itself increases. This has consequences for fire safety of the installation.

In addition, the maximum air cavity temperature approaches the ignition temperature of wood fibre insulation (100-130°C). While cellulose insulation (with approximately 8% fire retardant additives) ignite at higher temperatures between 250-400°C, as shown in table 1 (Chapter 3). Under a static external temperature of 35°C combined with solar radiation, an air cavity temperature of 106.3°C was reached. When dynamic temperature input was applied, the maximum cavity temperature reached 80.7°C. The static temperature scenario does not fully represent the Dutch climate, because it is unlikely that a constant outdoor temperature of 35°C will occur for longer periods. However, the dynamic temperature input derived from climate measurements in De Bilt may underestimates extreme conditions. The closer the cavity temperature approaches the ignition temperature of the material, the less additional energy is required to initiate ignition.

5.1. Assumptions in Voltra

The simulation was based on several assumptions and existing measurement data and literature sources. These factors influenced the outcome of the results:

5.1.1. Dynamic temperature input

The two scenarios implemented in the Voltra simulation were based on climate measurement data from the De Bilt. This data does not represent a worst-case scenario, as higher solar radiation levels and temperatures have been measured in other places in the Netherlands. Nevertheless, the dataset is accurate and provide a valuable insight into realistic environmental conditions. For a follow-up study, it would be valuable to investigate whether the maximum temperature and solar radiation measured in the Netherlands can be translated into dynamic input data, which would allow for a more conservative scenario.

5.1.2. Convection coefficient

For the convection coefficient between the exterior surface and the outdoor air, a recommended value of 13.5 W/m²K, provided by the software developer, was applied to represent a worst-case scenario with limited wind exposure. Under conditions with even lower wind speeds, the convection coefficient may be even lower. In such cases, the roof would be less capable of dissipating heat, potentially resulting in higher temperatures in the cavity than those predicted in the simulation.

5.1.3. Simulation set-up

In the simulation, an air cavity of 45 mm was assumed, based on commonly used battens and framing dimensions in the Netherlands. In practice, this cavity thickness may vary. Variations in the cavity width can influence the heat transfer by convection and conduction, potentially resulting in temperature differences compared to values obtained in this study. This study focused exclusively on the influence of the insulation material on the temperature in the air cavity. As a result, only the insulation material was modified, both in terms of its thermal properties and thickness, to achieve an insulation value of 6.3 m²K/W. Other roof elements were maintained constant.

5.2. Limitations of this study

This study has limitations that may affect the accuracy of the results.

5.2.1. Air cavity ventilation

Despite the questions posed to the software engineer, it is possible that certain functions of the programme were not used to their full potential. An attempt was made to iteratively determine the air flow occurring within the air cavity at elevated temperatures using the VVMOD program. However, it was not possible to implement the calculated airflow rates in the Voltra model. Ventilation within the air cavity could only be simulated as airflow entering perpendicular to the roof surface from the exterior, whereas the chimney effect which may occur at elevated temperatures and is characterised by the airflow parallel to the insulation surface, could not be reproduced. As a result, the simulated air cavity temperatures are likely higher than those that would occur in practice, where the chimney effect would provide additional cooling of the cavity.

5.2.2. Roof structure

This study assumed that the PV panels were integrated into the roof structure, with the insulation material located behind a defined air cavity. In practice, certain installation components may be closer to the insulation material than assumed in the simulation. Such variations in the construction may influence temperature development within the air cavity. In addition, no sheet material was included in the model as a protective layer between the PV panels and the underlying insulation. The presence of such a shielding layer could reduce heat transfer toward the insulation material and may result in lower temperatures at the exterior surface of the insulation material.

5.2.3. PV efficiency

The literature review indicates that the efficiency of PV panels decreases as air temperature increases. In this study, the additional heat production resulting from reduced efficiency of the PV panels was not included in the simulations. The simulated temperatures in the air cavity may be slightly lower than those that would occur if the heat generation of the PV panels were taken into account.

5.3. Recommendations for further research

For future research, it is recommended to investigate the influence of the air cavity thickness and the air cavity flow on the temperature at the exterior surface of the insulation material. In the current model, the roof battens and counter battens are not included in the simulation, which has an influence on the airflow and friction loss in case of a ventilated cavity.

Experimental testing or simulating fire scenarios could provide further insights into the fire behaviour of different insulation materials underneath BIPV panels. Performing field measurements under BIPV installations could also provide valuable data for comparison between measured temperatures and those predicted by the simulated scenarios. In addition, it would be beneficial to assess the impact of elevated temperatures on PV panels in both the long- and short-term periods and to relate these effects to potential fire risks. Beside this the extreme temperature data should be incorporated in a dynamic temperature load and their effect on air cavity temperatures.

6. Conclusion

The main objective of this study was to investigate the influence of bio-based insulation materials on fire safety and temperature development in an unventilated air cavity under a sloping roof with BIPV panels.

The simulations showed that the choice of insulation material influenced the temperature development in the air cavity. Bio-based insulation materials, due to their high heat capacity, result in slightly lower air cavity temperatures, whereas PIR insulation resulted in the highest air cavity temperatures. However, the temperature difference between bio-based and traditional insulation materials remains limited, at approximately 4°C.

Overall, the results indicate that bio-based insulation materials with a low ignition temperature reduce the fire safety of the air cavity. Especially at the elevated temperatures that can develop within the air cavity, small ignition sources can trigger combustion, increase the fire risk within the air cavity.

Wood fibre insulation, with an ignition temperature of 100-130°C, was the only insulation material in this study that approached the calculated air cavity temperatures. The simulation in which the temperature exceeded 100°C was based on a constant external air temperature of 35°C. Although possible peak outdoor temperatures may temporarily exceed this constant temperature, it provides a conservative estimation. Dynamic simulations based on temperature measurements in De Bilt can be too optimistic, as higher external temperatures can occur elsewhere in the Netherlands. Therefor cavity temperatures exceeding 85°C can be considered realistic under extreme summer conditions. Other insulation materials included in this study have an ignition temperature of at least 250°C, as can be seen in Table 1 (Chapter 3). The closer the cavity temperature approaches the ignition temperature of the material, the less additional energy is required to initiate ignition.

Based on these findings, the unprotected use of wood fibre insulation in the air cavity requires careful consideration. The increased temperature in the air cavity due to the external temperature and solar radiation may lead to thermal hotspots and malfunctions in the PV-panel, thereby increasing the risk of fire.

This study contributes to the understanding of temperatures development underneath BIPV panels, particularly in relation to bio-based insulation materials. The findings of this research highlight the importance of careful material use, especially when combustible materials with low ignition temperatures are used. Besides the material selection, this research underlines the beneficial effect of ventilation under PV-panels, as ventilation enhances heat dissipation and improves the efficiency.

Further research is recommended, particularly field measurements under BIPV to compare measured temperatures with simulation results. This could be combined with research into the efficiency of the PV panels when the temperature rises. In addition, further simulation research is recommended to investigate the influence of the air cavity thickness on the temperature at the exterior surface of the insulation material. Beside this the extreme temperature data should be incorporated in a dynamic temperature load and their effect on air cavity temperatures.

References

AgentschapNL. (2011). *Gebouw integratie zonnestroomsystemen Praktijkvoorbeelden van succesvolle producten*. https://www.rvo.nl/sites/default/files/bijlagen/Gebouwintegratie%20zonnestroomsystemen.pdf

Circle Economy. (2025). *The circularity gap report 2025*. https://circulars.iclei.org/wp-content/uploads/2025/06/CGR-2025-Report-compressed.pdf

Clarion Events North America. (2000, November 1). *HOW TO AVOID REKINDLES*.

E.E. Bende, & N.J.J. Dekker. (2019). *Brandincidenten met fotovoltaïsche (PV) systemen in Nederland. Een inventarisatie*. https://publications.tno.nl/publication/34633946/bhxqSn/TNO-2019-R10287.pdf

Giunta d'Albani, A. W., de Kluiver, L. L., de Korte, A. C. J., van Herpen, R. A. P., Weewer, R., & Brouwers, H. J. H. (2017). Mass loss and flammability of insulation materials used in sandwich panels during the pre-flashover phase of fire. *Fire and Materials*, *41*(6), 779–796. https://doi.org/10.1002/fam.2418

Godakandage, R., Weerasinghe, P., Gamage, K., Adnan, H., & Nguyen, K. (2023). A Systematic Review on Cavity Fires in Buildings: Flame Spread Characteristics, Fire Risks, and Safety Measures. In *Fire* (Vol. 7, Number 1). Multidisciplinary Digital Publishing Institute (MDPI). https://doi.org/10.3390/fire7010012

Hemann Laukamp, Georg Bopp, Robin Grab, Christof Wittwer, Heinrich Häberlin, Bettina van Heeckeren, Severin Phillip, Florian Reill, Heribert Schmidt, Annett Sepanski, Horst Thiem, & Willi Vaassen. (2013). *PV FIRE HAZARD - ANALYSIS AND ASSESSMENT OF FIRE INCIDENTS*. https://www.ise.fraunhofer.de/content/dam/ise/de/documents/publications/conference-paper/28-eupvsec-2013/Laukamp_5BV771.pdf

Ir. H.G. Krijgsman, & Ir. R.H.G. Roijakkers. (2021). *Rapportage Impactstudie zonnepanelen op daken*. https://profinrg.nl/wp-content/uploads/2024/05/Impactstudiezonnepanelenopdaken.pdf

J. Reinders, J. van der Graaf, M. Duyvis, & M. Leene. (2023). *Duurzaam bouwen-brandveiligheid van installaties*. https://nipv.nl/wp-content/uploads/2023/04/20230406-NIPV-Duurzaam-bouwen-brandveiligheid-van-installaties.pdf

KNMI. (2025). *Meer zon, maar niet door draaiende wind*. https://www.knmi.nl/over-het-knmi/nieuws/knmi-klimaatbericht-solar-radiation-trend-netherlands-toename-zonnestraling-nederland

Lente-Akkoord Circulair Industrieel Bouwen. (2024). *Eenvoudig toepasbare biobased isolatie-materialen*. https://www.lente-akkoord.nl/uploads/Lente-Akkoord-Eenvoudig-toepasbare-biobased-isolatie-materialen-2-25.3.pdf

Maksym Li, Prabhakar M. N., Jong-kyu Park, & Jung-il Song. (2025). *Flame-retardant innovations in bio-based treatments for lignocellulosic natural fibers: A review*. https://www.sciencedirect.com/science/article/abs/pii/S0141813025042801

Nederlands Instituut Publieke Veiligheid. (2025). *Kennisdocument Zonnepanelen*. https://nipv.nl/wp-content/uploads/2025/06/20250501-VRU-NIPV-Kennisdocument-zonnepanelen.pdf

NEN. (2012, March 1). *NEN 1068*.

NEN. (2019a). *NEN 6063*. https://connect.nen.nl/Standard/PopUpHtml?RNR=3618015&search=&Native=1&token=59073259-8cde-4609-b14e-35ba4009a641

NEN. (2019b, January 1). *NEN-EN 13501-1:2019 en*. NEN.

NEN. (2022). *NEN 6069*. https://connect.nen.nl/Standard/PopUpHtml?RNR=3675466&search=&Native=1&token=2359b0de-08d4-4ccf-83f4-81bf40f6b085

R. van Herpen. (2022, January 28). *Webinar: PV panelen en brandrisico's*.

R. van Liempd, P. van Rede, & L. De Witte. (2024). *Introductie doelgerichte brandveiligheid*. https://nipv.nl/wp-content/uploads/2024/11/20241108-NIPV-Introductie-doelgerichte-brandveiligheid.pdf

RVO. (2022). *Onderzoek brandveiligheid van biobased isolatiematerialen in houtachtige elementen*. https://circulairebouweconomie.nl/wp-content/uploads/2022/12/Technisch-rapport-Brandveiligheid-biobased-bouwmaterialen_def_002.pdf

S. Baaij, L. de Witte, R. Hofman, E. Huizer, J. Molenaar, & R. Weewer. (2023). *Handboek gebouwbrandbestrijding*. https://nipv.nl/wp-content/uploads/2023/03/20230123-NIPV-Handboek-Gebouwbrandbestrijding.pdf

Sudhoff, P. (2024). *Modeling the Fire Behavior of Bio-Based Insulation Materials*. https://www.researchgate.net/profile/Patrick-Sudhoff/publication/381323627_Modeling_the_Fire_Behavior_of_Bio-Based_Insulation_Materials/links/66699e00a54c5f0b9460cb5e/Modeling-the-Fire-Behavior-of-Bio-Based-Insulation-Materials.pdf

Thijs van Druenen. (2025). *Department of the Built Environment Thijs van Druenen*. https://canvas.tue.nl/courses/29366/pages/ham-week-1?module_item_id=641127

Veiligheidsregio Haaglanden. (2024). *“Wet- en regelgeving levert niet automatisch een brandveilig gebouw op” _ Veiligheidsregio Haaglanden*. https://www.vrh.nl/nieuws-verhalen/verhalen/wet-en-regelgeving-levert-niet-automatisch-een-brandveilig-gebouw-op

Velds, C. A. . (1992). *Zonnestraling in Nederland*. Koninklijk Nederlands Meteorologisch Instituut. https://cdn.knmi.nl/knmi/pdf/bibliotheek/knmipubDIV/Zonnestraling_in_Nederland.pdf

Zhang, Y., Xu, J., Mao, J., Tao, J., Shen, H., Chen, Y., Feng, Z., Verlinden, P. J., Yang, P., & Chu, J. (2015). Long-term reliability of silicon wafer-based traditional backsheet modules and double glass modules. *RSC Advances*, *5*(81), 65768–65774. https://doi.org/https://www.researchgate.net/publication/280631423_Long-term_reliability_of_silicon_wafer-based_traditional_backsheet_modules_and_double_glass_modules

Declaration of generative AI and AI-assisted technologies in the writing process

I acknowledge the use of generative artificial intelligence in the preparation of this report. I utilized ChatGPT to improve the linguistic quality of the text. The prompts used included “Rewrite the following text in formal academic English and improve my grammar.”. The output from these prompts was used to enhance readability and to correct grammatical errors. After using ChatGPT, the author reviewed and edited the content as needed and take full responsibility for the content of the publication.

Appendix

Appendix 1

Analytical temperature calculation

Temperature at the exterior surface

The external surface of the structure is heated by the air temperature and solar radiation. The external surface temperature of the structure is determined using equation 01.

$$e * q_{rad} + h_a * (T_a - T_{ao}) - \frac{T_{ao} - T_{io}}{R_c} - h_i(T_{io} - T_i) = 0 \quad (01)$$

Where:

$e = absorption\ factor\ [-]$
$q_{rad} = irradiance\ [W/m^2]$
$h_a = external\ heat\ transfer\ coefficient\ [W/m^2K]$
$T_a = external\ temperature\ [°C]$
$T_{ao} = exterior\ surface\ temperature\ [°C]$
$h_i = internal\ heat\ transfer\ coefficient\ [W/m^2K]$
$T_i = internal\ temperature\ [°C]$
$T_{io} = interior\ surface\ temperature\ [°C]$
$R_c = thermal\ resistance\ of\ the\ construction\ [m^2K/W]$

Thermal resistance of the construction

The thermal resistance of the materials was determined based on their thickness and thermal conductivity using equation 04. The thermal conductivity, thickness, and the calculated thermal resistance of each layer is presented in Table 2.

$$R = \frac{d}{\lambda} \quad (04)$$

Where:

$R = thermal\ resistance\ [m^2K/W]$

$d = thickness\ [m]$

$\lambda = thermal\ conductivity\ [W/mK]$

Table 4: Materials and thermal conductivity

	Thermal conductivity λ [W/(mK)]	Thickness [mm]	Rd [m²K/W]
integrated pv panels	1.000	40	0.040
cavity (unventilated)	0.212	36	0.170
wood fibre insulation	0.042	265	6.310
wood	0.170	18	0.106

The total thermal resistance of the construction is calculated with the sum of all materials within the construction.

$$R_c = 6.63\ m^2K/W$$

Steady state heat transfer

A steady-state condition is assumed, in which the heat flow through the construction equals the heat flow leaving the construction.

$$\frac{T_{ao} - T_{io}}{R_c} = h_i(T_{io} - T_i) \quad (05)$$

$h_i = 7.7\ W/m^2K$
$T_i = 30°C$
$R_c = 6.63\ m^2K/W$

The equation is rearranged to express T_{oa}as a function of T_{io}:

$$T_{ao} = 51.96Tio + 1528.94$$

Calculation of the exterior surface temperature

The temperatures of the external structure (T_{oa}) and the internal structure (T_{io}) were determined by substitution.

$$e * q_{rad} + h_a * (T_a - T_{ao}) - \frac{T_{ao} - T_{io}}{R_c} - h_i(T_{io} - T_i) = 0$$

$e = 0.9$
$q_{rad} = 1000\ W/m^2$
$h_a = 13.5\ W/m^2K$
$T_a = 35\ °C$
$T_{ao} = 51.96Tio + 1019.29$
$h_i = 7.7\ W/m^2K$
$T_i = 30°C$
$R_c = 6.63\ m^2K/W$

$$T_{io} = 31.39°C$$
$$T_{ao} = 100.11°C$$

Heat flux through the construction

The heat flux through the construction is determined using equation 02.

$$q = \frac{(T_{oa} - T_{io})}{R_c} \quad (02)$$

$T_{oa} = 100.11°C$
$T_{io} = 31.39°C$
$R_c = 6.63\ m^2K/W$

$$q = 10.37\ W/m^2$$

Temperature at the outside of the insulation layer

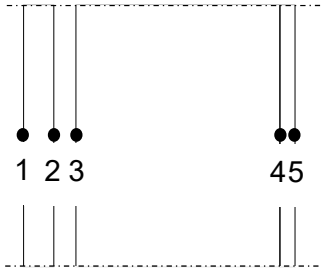

Figure 13: Schematic representation of the construction layers from the exterior to the interior.

At the outside of the insulation material (junction 3, as can be seen in figure 2), the temperature is determined using equation 03. For this calculation, the thermal resistances of the layers up to this junction (determined in table 2) are summed.

$$T_{outside\ inulation} = T_{ao} - q * \sum_{i=3}^{j} R \qquad (03)$$

$T_{oa} = 100.11°C$
$q = 10.37\ W/m^2$
$\sum_{i=3}^{j} R = 0.284\ m^2K/W$

$$T_{outside\ inulation} = 97.2°C$$

Appendix 2a

Table 5: Percentiles of hourly sums in Wh/m² of global radiation at De Bilt for different hourly periods of the day

hour / month	4	5	6	7	8	9	10	11	12	13	14	15	16	17	18	19	20	21
January	0	0	0	0	6	103	228	303	350	342	294	200	78	0	0	0	0	0
February	0	0	0	6	117	275	400	489	531	525	469	369	231	69	0	0	0	0
March	0	0	14	150	333	478	617	689	722	703	636	531	383	228	61	0	0	0
April	0	19	142	308	469	628	736	831	842	819	783	664	514	361	192	36	0	0
May	3	97	247	406	564	703	819	886	917	900	833	736	611	444	303	136	14	0
June	8	114	269	431	589	728	833	906	911	917	869	772	653	500	325	167	28	0
July	6	108	250	403	581	692	822	889	906	900	864	767	636	481	333	175	28	0
August	0	36	161	317	481	614	706	833	850	819	781	678	542	400	261	108	3	0
September	0	0	58	231	408	528	619	700	744	761	639	583	450	256	100	6	0	0
October	0	0	0	89	242	381	494	597	592	553	514	369	239	92	0	0	0	0
November	0	0	0	3	86	214	311	386	394	386	278	169	61	0	0	0	0	0
December	0	0	0	0	6	94	194	239	289	253	181	86	3	0	0	0	0	0

Appendix 2b

table 6: Percentiles of hourly totals in Wh/m² of global radiation at De Bilt for different hourly periods of the day. With a safety margin of 15% for the increase in solar radiation over the past 35 years.

hour / month	4	5	6	7	8	9	10	11	12	13	14	15	16	17	18	19	20	21
January	0	0	0	0	6	118	262	348	403	393	339	230	89	0	0	0	0	0
February	0	0	0	6	134	316	460	562	610	604	540	425	265	80	0	0	0	0
March	0	0	16	173	383	549	709	792	831	808	732	610	441	262	70	0	0	0
April	0	22	163	355	540	722	847	955	968	942	901	763	591	415	220	42	0	0
May	3	112	284	466	648	808	942	1019	1054	1035	958	847	703	511	348	157	16	0
June	10	131	310	495	677	837	958	1041	1048	1054	1000	888	751	575	374	192	32	0
July	6	125	288	463	668	795	946	1022	1041	1035	993	882	732	553	383	201	32	0
August	0	42	185	364	553	706	811	958	978	942	898	779	623	460	300	125	3	0
September	0	0	67	265	470	607	712	805	856	875	735	671	518	294	115	6	0	0
October	0	0	0	102	278	438	569	687	680	636	591	425	275	105	0	0	0	0
November	0	0	0	3	99	246	358	444	454	444	319	195	70	0	0	0	0	0
December	0	0	0	0	6	109	224	275	332	291	208	99	3	0	0	0	0	0

Appendix 3

Day	Time	Temperature [°C]	Solar radiation global [W/m²]	Solar radiation diffuse [W/m²]	Solar beam radiation [W/m²]	Long wave radiation [W/m²]	wind speed [m/s]
230.0	1.0	24.5	0.0	0.0	0.0	386.0	0.5
230.0	2.0	23.9	0.0	0.0	0.0	376.0	0.6
230.0	3.0	23.9	0.0	0.0	0.0	377.0	0.5
230.0	4.0	23.8	0.0	0.0	0.0	377.0	0.1
230.0	5.0	24.0	0.0	0.0	0.0	378.0	0.2
230.0	6.0	23.7	0.0	0.0	0.0	377.0	0.5
230.0	7.0	24.8	26.0	25.0	14.0	383.0	0.3
230.0	8.0	26.1	222.0	44.0	674.0	389.0	0.9
230.0	9.0	27.4	422.0	49.0	835.0	396.0	1.1
230.0	10.0	28.8	595.0	90.0	829.0	403.0	1.1
230.0	11.0	30.2	766.0	113.0	881.0	410.0	1.2
230.0	12.0	30.9	893.0	92.0	962.0	414.0	1.1
230.0	13.0	32.3	956.0	98.0	978.0	421.0	2.2
230.0	14.0	32.5	948.0	98.0	974.0	422.0	2.6
230.0	15.0	33.0	876.0	90.0	958.0	424.0	3.8
230.0	16.0	33.3	737.0	81.0	909.0	425.0	3.8
230.0	17.0	31.9	574.0	83.0	841.0	418.0	2.6
230.0	18.0	30.1	406.0	65.0	817.0	407.0	2.9
230.0	19.0	29.2	193.0	44.0	643.0	402.0	3.1
230.0	20.0	27.8	28.0	26.0	51.0	394.0	3.1
230.0	21.0	26.7	0.0	0.0	0.0	396.0	2.2
230.0	22.0	26.1	0.0	0.0	0.0	392.0	1.5
230.0	23.0	26.0	0.0	0.0	0.0	399.0	1.7
230.0	24.0	25.3	0.0	0.0	0.0	395.0	1.9

Appendix 4a

VOLTRA data file: Voltra steady state simulation

GRID

No.	X [mm]	Y [mm]	Z [mm]
0-1	1000.000	1000.000	500.000
1-2	1000.000	1000.000	2.000
2-3			3.000
3-4			4.000
4-5			4.000
5-6			3.000
6-7			2.000
7-8			2.000
8-9			3.000
9-10			4.500
10-11			6.750
11-12			10.125
12-13			15.188
13-14			22.781
14-15			34.172
15-16			33.984
16-17			33.984
17-18			34.172
18-19			22.781
19-20			15.188
20-21			10.125
21-22			6.750
22-23			4.500
23-24			3.000
24-25			2.000
25-26			20.000
26-27			25.000
27-28			2.000
28-29			3.000
29-30			4.500
30-31			6.750
31-32			3.750
32-33			3.750
33-34			6.750
34-35			4.500
35-36			3.000
36-37			2.000
37-38			500.000
Sum	2000.000	2000.000	1368.000

BLOCKS

No.	Col.	Xmin	Xmax	Ymin	Ymax	Zmin	Zmax
1	0	0	2	0	2	27	37
2	1	0	2	0	2	37	38
3	2	0	2	0	2	25	26
4	2	0	2	0	2	26	27
5	3	0	2	0	2	0	1
6	7	0	2	0	2	7	25
7	108	0	2	0	2	1	7

No.	Col.	Xmin	Xmax	Ymin	Ymax	Zmin	Zmax
1	0	0.000	2000.000	0.000	2000.000	828.000	868.000
2	1	0.000	2000.000	0.000	2000.000	868.000	1368.000
3	2	0.000	2000.000	0.000	2000.000	783.000	803.000

4	2	0.000	2000.000	0.000	2000.000	803.000	828.000
5	3	0.000	2000.000	0.000	2000.000	0.000	500.000
6	7	0.000	2000.000	0.000	2000.000	518.000	783.000
7	108	0.000	2000.000	0.000	2000.000	500.000	518.000

FUNCTIONS

COLOURS

Col.	Type	CEN-rule	Name	lambda	eps	rho	c	t	h	q
				[W/mK]	[-]	[kg/m3]	[J/kgK]	[°C]	[W/m²K]	[W/m²]
0	MATERIAL		PV	1.000	0.90	1500.0	1500.0			
1	BC_SIMPL	NIHIL	outside air					35.0	13.50	1000
2	BC_FREE	CEN_Zy_I	cavity			1.2	1000.0			
3	BC_SIMPL	HI_NORML	inside air					30.0	7.70	0
7	MATERIAL		insulation	0.042	0.90	40.0	2100.0			
108	MATERIAL		fibreboard	0.170	0.90	700.0	1880.0			

Col.	ta	hc	Pc	tr	C1	C2	C3	Sun	rs	ts
	[°C]	[W/m²K]	[W]	[°C]	[-]	[-]	[-]		[-]	[-]
0									0.10	0.00
1								NO		
2		1.11	0		0.025	0.352	0.187			
3								NO		
7									0.10	0.00
108									0.10	0.00

NODE BC-S

No.	X	Y	Z	Type	t	P
					[°C]	[W]
1	1	1	25	POWER		0
2	1	1	27	POWER		0

OUTPUT NODES

No.	X	Y	Z
1	1	1	25
2	1	1	27

Calculation parameters

Time step interval = 0000:01:00:00
Start-up calculation duration = 0000:00:00:00
Calculation duration = 0001:00:00:00
Day number at start of calculation = 1
Maximum number of iterations = 10000
Maximum temperature difference = 0.01°C
Heat flow divergence for total object = 1 %
Heat flow divergence for worst node = 1 %
Linear radiation
Smallest accepted view factor = 0.0001
Number of visibility rays between radiative surfaces = 100
Black radiation heat transfer coeff. = 5.25 W/(m².K)
Default temperature difference across airspace = 10°C

Appendix 4b

VOLTRA data file: Voltra scenario 1

GRID

No.	X [mm]	Y [mm]	Z [mm]
0-1	1000.000	1000.000	500.000
1-2	1000.000	1000.000	2.000
2-3			3.000
3-4			4.000
4-5			4.000
5-6			3.000
6-7			2.000
7-8			2.000
8-9			3.000
9-10			4.500
10-11			6.750
11-12			10.125
12-13			15.188
13-14			22.781
14-15			34.172
15-16			33.984
16-17			33.984
17-18			34.172
18-19			22.781
19-20			15.188
20-21			10.125
21-22			6.750
22-23			4.500
23-24			3.000
24-25			2.000
25-26			20.000
26-27			25.000
27-28			2.000
28-29			3.000
29-30			4.500
30-31			6.750
31-32			3.750
32-33			3.750
33-34			6.750
34-35			4.500
35-36			3.000
36-37			2.000
37-38			500.000
Sum	2000.000	2000.000	1368.000

BLOCKS

No.	Col.	Xmin	Xmax	Ymin	Ymax	Zmin	Zmax
1	0	0	2	0	2	27	37
2	1	0	2	0	2	37	38
3	2	0	2	0	2	25	26
4	2	0	2	0	2	26	27
5	3	0	2	0	2	0	1
6	7	0	2	0	2	7	25
7	108	0	2	0	2	1	7

No.	Col.	Xmin	Xmax	Ymin	Ymax	Zmin	Zmax
1	0	0.000	2000.000	0.000	2000.000	828.000	868.000
2	1	0.000	2000.000	0.000	2000.000	868.000	1368.000
3	2	0.000	2000.000	0.000	2000.000	783.000	803.000

```
4       2        0.000  2000.000     0.000  2000.000   803.000   828.000
5       3        0.000  2000.000     0.000  2000.000     0.000   500.000
6       7        0.000  2000.000     0.000  2000.000   518.000   783.000
7     108        0.000  2000.000     0.000  2000.000   500.000   518.000

FUNCTIONS
G01: FILE
  C:\Users\kimbe\Downloads\2DeBilt_MN4.FSG
D01: FILE
  C:\Users\kimbe\Downloads\3DeBilt_MN4.FSD

COLOURS
Col. Type       CEN-rule  Name               lambda      eps     rho        c
t       h       q
                                           [W/mK]        [-]  [kg/m3]  [J/kgK]
[°C] [W/m²K]  [W/m²]
  0  MATERIAL            PV                1.000    0.90  1500.0  1500.0
  1  BC_SIMPL  NIHIL     outside air                                    35.0
13.50       0
  2  BC_FREE   CEN_Zy_I  cavity                                   1.2  1000.0
0
  3  BC_SIMPL  HI_NORML  inside air                                    30.0
7.70       0
  7  MATERIAL            insulation        0.042    0.90    40.0  2100.0
108  MATERIAL            fibreboard        0.170    0.90   700.0  1880.0

Col.     ta       hc       Pc       tr          C1         C2         C3     Sun
rs       ts
       [°C] [W/m²K]     [W]    [°C]       [-]        [-]        [-]              [-
]      [-]
  0                                                                          0.10
0.00
  1                                                                       YES
  2            1.11       0             0.025      0.352      0.187
  3                                                                       NO
  7                                                                          0.10
0.00
108                                                                          0.10
0.00

NODE BC-S
No.      X     Y     Z  Type          t          P
                                     [°C]      [W]
1        1     1    25  POWER                   0
2        1     1    27  POWER                   0

OUTPUT NODES
No.      X     Y     Z
1        1     1    25
2        1     1    27

SOLAR DATA
1. Rotation angle around Z axis = 0°
2. Rotation angle around X axis = 35°
3. Rotation angle around Z axis = 0°
Latitude = 52° N
Longitude = 0° E
Time zone = 2.8026e-45 h E
Horizontal global solar radiation function = G01
Horizontal diffuse solar radiation function = D01
Ground reflection factor = 0.20
```

SUN OBSTACLES

No.	Min. Azimuth [°]	Max. Azimuth [°]	Min. Altitude [°]	Max. Altitude [°]
1	-180	180	0	5

Calculation parameters

Time step interval = 0000:01:00:00
Start-up calculation duration = 0000:00:00:00
Calculation duration = 0001:00:00:00
Day number at start of calculation = 230
Maximum number of iterations = 10000
Maximum temperature difference = 0.01°C
Heat flow divergence for total object = 1 %
Heat flow divergence for worst node = 1 %
Linear radiation
Smallest accepted view factor = 0.0001
Number of visibility rays between radiative surfaces = 100
Black radiation heat transfer coeff. = 5.25 W/(m².K)
Default temperature difference across airspace = 10°C

Appendix 4c

VOLTRA data file: Voltra scenario 2

GRID

No.	X [mm]	Y [mm]	Z [mm]
0-1	1000.000	1000.000	500.000
1-2	1000.000	1000.000	2.000
2-3			3.000
3-4			4.000
4-5			4.000
5-6			3.000
6-7			2.000
7-8			2.000
8-9			3.000
9-10			4.500
10-11			6.750
11-12			10.125
12-13			15.188
13-14			22.781
14-15			34.172
15-16			33.984
16-17			33.984
17-18			34.172
18-19			22.781
19-20			15.188
20-21			10.125
21-22			6.750
22-23			4.500
23-24			3.000
24-25			2.000
25-26			20.000
26-27			25.000
27-28			2.000
28-29			3.000
29-30			4.500
30-31			6.750
31-32			3.750
32-33			3.750
33-34			6.750
34-35			4.500
35-36			3.000
36-37			2.000
37-38			500.000
Sum	2000.000	2000.000	1368.000

BLOCKS

No.	Col.	Xmin	Xmax	Ymin	Ymax	Zmin	Zmax
1	0	0	2	0	2	27	37
2	1	0	2	0	2	37	38
3	2	0	2	0	2	25	26
4	2	0	2	0	2	26	27
5	3	0	2	0	2	0	1
6	7	0	2	0	2	7	25
7	108	0	2	0	2	1	7

No.	Col.	Xmin	Xmax	Ymin	Ymax	Zmin	Zmax
1	0	0.000	2000.000	0.000	2000.000	828.000	868.000
2	1	0.000	2000.000	0.000	2000.000	868.000	1368.000
3	2	0.000	2000.000	0.000	2000.000	783.000	803.000

4	2	0.000	2000.000	0.000	2000.000	803.000	828.000
5	3	0.000	2000.000	0.000	2000.000	0.000	500.000
6	7	0.000	2000.000	0.000	2000.000	518.000	783.000
7	108	0.000	2000.000	0.000	2000.000	500.000	518.000

FUNCTIONS
T01: FILE
C:\Users\kimbe\Downloads\1DeBilt_MN4.FTE
G01: FILE
C:\Users\kimbe\Downloads\2DeBilt_MN4.FSG
D01: FILE
C:\Users\kimbe\Downloads\3DeBilt_MN4.FSD

COLOURS

Col.	Type	CEN-rule	Name	lambda	eps	rho	c	t	h	q
				[W/mK]	[-]	[kg/m3]	[J/kgK]	[°C]	[W/m²K]	[W/m²]
0	MATERIAL		PV	1.000	0.90	1500.0	1500.0			
1	BC_SIMPL	NIHIL	outside air					T01		
13.50	0									
2	BC_FREE	CEN_Zy_I	cavity			1.2	1000.0			
0										
3	BC_SIMPL	HI_NORML	inside air				30.0			
7.70	0									
7	MATERIAL		insulation	0.042	0.90	40.0	2100.0			
108	MATERIAL		fibreboard	0.170	0.90	700.0	1880.0			

Col.	ta	hc	Pc	tr	C1	C2	C3	Sun	rs	ts
	[°C]	[W/m²K]	[W]	[°C]	[-]	[-]	[-]		[-]	[-]
0									0.10	
0.00										
1								YES		
2		1.11	0		0.025	0.352	0.187			
3								NO		
7									0.10	
0.00										
108									0.10	
0.00										

NODE BC-S

No.	X	Y	Z	Type	t	P
					[°C]	[W]
1	1	1	25	POWER		0
2	1	1	27	POWER		0

OUTPUT NODES

No.	X	Y	Z
1	1	1	25
2	1	1	27

SOLAR DATA
1. Rotation angle around Z axis = 0°
2. Rotation angle around X axis = 35°
3. Rotation angle around Z axis = 0°
Latitude = 52° N
Longitude = 0° E
Time zone = 2.8026e-45 h E
Horizontal global solar radiation function = G01

Horizontal diffuse solar radiation function = D01
Ground reflection factor = 0.20

SUN OBSTACLES

No.	Min. Azimuth [°]	Max. Azimuth [°]	Min. Altitude [°]	Max. Altitude [°]
1	-180	180	0	5

Calculation parameters
Time step interval = 0000:01:00:00
Start-up calculation duration = 0000:00:00:00
Calculation duration = 0001:00:00:00
Day number at start of calculation = 230
Maximum number of iterations = 10000
Maximum temperature difference = 0.01°C
Heat flow divergence for total object = 1 %
Heat flow divergence for worst node = 1 %
Linear radiation
Smallest accepted view factor = 0.0001
Number of visibility rays between radiative surfaces = 100
Black radiation heat transfer coeff. = 5.25 W/(m².K)
Default temperature difference across airspace = 10°C